OPEN ACCESS

University of Dundee

University of Dundee

# Advanced titanium dioxide-polytetrafluorethylene (TiO2-PTFE) nanocomposite coatings on stainless steel surfaces with antibacterial and anti-corrosion properties

Zhang, Shuai; Liang, Xinjin; Gadd, Geoffrey Michael; Zhao, Qi

*Published in:*
Applied Surface Science

*DOI:*
10.1016/j.apsusc.2019.06.070

*Publication date:*
2019

*Licence:*
CC BY

*Document Version*
Publisher's PDF, also known as Version of record

Link to publication in Discovery Research Portal

*Citation for published version (APA):*
Zhang, S., Liang, X., Gadd, G. M., & Zhao, Q. (2019). Advanced titanium dioxide-polytetrafluorethylene (TiO2-PTFE) nanocomposite coatings on stainless steel surfaces with antibacterial and anti-corrosion properties. *Applied Surface Science*, *490*, 231-241. https://doi.org/10.1016/j.apsusc.2019.06.070

**General rights**
Copyright and moral rights for the publications made accessible in Discovery Research Portal are retained by the authors and/or other copyright owners and it is a condition of accessing publications that users recognise and abide by the legal requirements associated with these rights.

• Users may download and print one copy of any publication from Discovery Research Portal for the purpose of private study or research.
• You may not further distribute the material or use it for any profit-making activity or commercial gain.
• You may freely distribute the URL identifying the publication in the public portal.

**Take down policy**
If you believe that this document breaches copyright please contact us providing details, and we will remove access to the work immediately and investigate your claim.

Download date: 05. May. 2023

Applied Surface Science 490 (2019) 231–241

Contents lists available at ScienceDirect

Applied Surface Science

journal homepage: www.elsevier.com/locate/apsusc

Full length article

# Advanced titanium dioxide-polytetrafluorethylene ($TiO_2$-PTFE) nanocomposite coatings on stainless steel surfaces with antibacterial and anti-corrosion properties

Shuai Zhang[a], Xinjin Liang[b], Geoffrey Michael Gadd[b], Qi Zhao[a,*]

[a] School of Science & Engineering, University of Dundee, Dundee DD1 4HN, UK
[b] School of Life Sciences, University of Dundee, Dundee DD1 5EH, UK

ARTICLE INFO

*Keywords:*
Titanium dioxide
Polytetrafluoroethylene
Surface energy
Antibacterial activity
Corrosion

ABSTRACT

Bacterial infection and corrosion are two of the most common causes of the failure for the use of biomedical metallic implants. In this paper, we developed a facile two-step approach for synthesizing a $TiO_2$-PTFE nanocomposite coating on stainless steel substrate with both antibacterial and anticorrosion properties by using a sol-gel dip coating technique. A sub-layer of bioinspired polydopamine (PDA) was first coated on the stainless steel substrate to improve the adhesion and reactivity, then $TiO_2$-PTFE was uniformly co-deposited onto the PDA sub-layer. Both PTFE and $TiO_2$ contents had a significant influence on the surface energy of the $TiO_2$-PTFE coating. The coating with the total surface energy of 26 $mJ/m^2$ exhibited minimal bacterial adhesion against both Gram-negative *Escherichia coli* WT F1693 and Gram-positive *Staphylococcus aureus* F1557, which was explained using the extended DLVO theory. Benefiting from the synergistic effect between $TiO_2$ and PTFE, the $TiO_2$-PTFE coating showed improved corrosion resistance in artificial body fluids compared with the sole $TiO_2$ coating or PTFE coating. The TiO2-PTFE coating also demonstrated extraordinary biocompatibility with fibroblast cells in culture, making it a prospective strategy to overcome current challenges in the use of metallic implants.

## 1. Introduction

Metallic implants are engineered systems designed to provide internal support to biological tissues and have been used extensively in dental, endovascular and orthopaedic surgery [1,2]. However, the high incidence of medical implant-related infections and complications are associated with increased morbidity and mortality, prolonged hospitalisation, patient discomfort and increased medical costs. Bacteria can adhere to implant surfaces and become embedded in a dense extracellular matrix which shields the bacteria from host defence mechanisms and blocks antibiotic penetration [3,4]. Despite extensive local tissue debridement and prolonged systemic and targeted local antimicrobial therapy, the infected device often must be removed to fully resolve the problem [5]. Current strategies for preventing infections include coating or impregnating antibacterial agents such as antibiotics [6], nano-silver [7] and other antiseptics [8,9] onto the implant surface. However, most of these attempts fail to deliver sustained antibacterial effects as the coatings are prone to loss of activity after covalent bonding [10]. Microbes being exposed to sub-lethal levels of the antimicrobials may trigger the emergence of resistance in situ. Silver has been documented to possess a broad spectrum of antimicrobial activity, but there are certain concerns about its cytotoxicity towards mammalian cells [11]. Antibacterial polymer or peptides have also been accepted as promising candidates to impart device surfaces with antibacterial properties, although, problems such as poor adherence and the risk of polymer degradation-induced inflammatory responses still exist [12].

In addition to the above problems, the long-term presence of metal devices in the body is associated with an increased risk of corrosion which can significantly undermine the long-term performance of implants and lead to an increase in inflammatory responses [13,14]. For instance, previous studies have shown that 316L stainless steel (316L SS) implants are often subject to degradation due to pitting, crevice formation, corrosion fatigue, fretting corrosion, stress corrosion cracking and galvanic corrosion in the body [15]. Released cytotoxic constituents such as nickel and chromium ions are accumulated in the tissues surrounding the implants and can migrate through the blood to be accumulated in vital organs such as the kidney, spleen and liver [16]. Therefore, designing a novel coating for metallic implants with long-term efficient antibacterial and anti-corrosion activities would be

* Corresponding author.
*E-mail address:* q.zhao@dundee.ac.uk (Q. Zhao).

https://doi.org/10.1016/j.apsusc.2019.06.070
Received 28 February 2019; Received in revised form 25 May 2019; Accepted 7 June 2019
0169-4332/ © 2019 The Authors. Published by Elsevier B.V. This is an open access article under the CC BY license (http://creativecommons.org/licenses/by/4.0/).

an important strategy to cope with these issues.

Titanium dioxide ($TiO_2$) represents a type of broad-spectrum bactericide with excellent biocompatibility and corrosion resistance [17–20]. Activation of $TiO_2$ particles with adequate UV light generates electrons and holes that react with adsorbed water and dioxygen molecules to form reactive oxygen species (ROS), killing or inhibiting the growth of bacteria by penetrating their cell walls [21,22]. Ohko et al. [23] reported that silicone catheters coated with $TiO_2$ photocatalyst thin films exhibited a strong bactericidal effect under UV illumination. Moreover, numerous studies have demonstrated that the inclusion of $TiO_2$ in coatings can result in a correlated change in surface energy and its components, which has a significant influence on bacterial adhesion [24–26]. Zhao et al. [27] incorporated $TiO_2$ nanoparticles into Ni-P coatings and found that the electron donor surface energy ($\gamma^-$) of the Ni-P-$TiO_2$ coatings increased significantly with increasing $TiO_2$ content after UV irradiation. They also found that the number of adhering bacteria decreased with increasing electron donor surface energy of the coatings. These studies indicated that employing $TiO_2$ in coatings could produce a self-sterilizing surface with both antibacterial and anti-adhesive properties after ultraviolet illumination.

Recently, Liu and Zhao [28] demonstrated that the ratio of the Lifshitz-van der Waals (LW) apolar component to electron donor surface-energy components of substrates ($\gamma^{LW}/\gamma^-$, also called the CQ ratio) controls bacterial adhesion. They found that surfaces with the lowest CQ ratio had the lowest bacterial adhesion. Polytetrafluorethylene (PTFE) is a well-recognised biomaterial with low surface energy and numerous studies have shown that the incorporation of PTFE nanoparticles into the metallic matrix significantly reduced the $\gamma^{LW}$ component of the coatings, which is one of the main reasons for the coatings to have non-stick or antibacterial properties [29–31]. However, no research has been reported on the antibacterial properties of $TiO_2$-PTFE nanocomposite coatings. In this paper, we aimed for the first time to develop a $TiO_2$-PTFE nanocomposite coating to protect 316 L stainless steel implants from bacterial infection and corrosion. Firstly, we applied the mussel-inspired polymer coating strategy to functionalise the stainless steel substrate with catechol groups which could be a platform for secondary reactions to deposit $TiO_2$ sols [32]; $TiO_2$-PTFE coatings were then prepared via a facile sol-gel technique. The antibacterial and anti-adhesion efficiencies of the coatings were evaluated with both Gram-negative (*Escherichia coli*) and Gram-positive (*Staphylococcus aureus*) bacterial strains. Anti-corrosion properties were assessed using an electrochemical method. Biocompatibility at the mammalian cell level was also evaluated.

## 2. Materials and methods

### 2.1. Preparation of $TiO_2$-PTFE nanocomposite coatings

Commercially available 316 L stainless steel plates (25 mm × 25 mm × 1 mm) were cleaned by ultrasonication in ethanol and deionised water, respectively. The mussel-inspired strategy to prepare polydopamine sublayer onto the surface of 316L stainless steel, and the sol-gel process to prepare $TiO_2$-PTFE nanocomposite coatings are illustrated in Fig. 1a. In brief, prior to $TiO_2$-PTFE sol-gel coating, the plates were treated with 2 mg/mL dopamine (Sigma-Aldrich, UK) in 10 mM Tris-HCl buffer (10 mM, pH = 8.5, Sigma-Aldrich, UK) for 24 h under constant stirring at 100 rpm at 25 °C [33]. A $TiO_2$ precursor sol was prepared via the acid catalysed controlled hydrolysis of titanium (IV) butoxide (TBOT) (Sigma-Aldrich, UK) in ethanol (EtOH) (Sigma-Aldrich, UK). In this study, 0.1 M nitric acid ($HNO_3$) (Sigma-Aldrich, UK) was used as a catalyst and the volume ratio for TBOT: EtOH: 0.1 M $HNO_3$ was 1: 40: 2. Then 1.0–2.0 g/L $TiO_2$ nanoparticles (anatase, < 25 nm, Sigma-Aldrich, UK) and 2.0 g/L of PTFE particles with a mean particle size of 200–300 nm (Polysciences, Inc., USA) were introduced into the sol and thoroughly mixed by ultrasonication. The mixture was further left with continuous stirring at room temperature for 24 h to allow complete hydrolysis and condensation of TBOT. Prior to the dip coating process, the sub-coated plates were ultrasonicated and rinsed with deionised water to detach excess monomer and particles. The plates were then vertically immersed into the mixture for 30s and withdrawn at a constant speed of 5 mm/s. After each coating, the plate was air dried at room temperature and rinsed 3 times with ethanol to remove excess TBOT and $TiO_2$. Finally, the coated plates were heat-treated at 100 °C for 2 h with a heating rate of 2 °C $min^{-1}$ in all cases.

### 2.2. Surface characterisation

The surface morphology of the coatings was characterised using scanning electron microscopy (Field emission-scanning electron microscope (FE-SEM), JEOL JSM-7400F, Tokyo, Japan) with an accelerating voltage of 5 kV and atomic force microscope (AFM, Dimension 3000, Santa Barbara, CA, U.S.A.). The particle size distribution was calculated from random SEM images for triplicate specimens using ImageJ software. For surface composition analysis, energy-dispersive X-ray spectrometry (EDX, QX200, Bruker, Billerica, U.S.A.) and UHV X-ray photoemission (XPS, ESCALAB 250, Waltham, U.S.A.) were used. The distributions of $TiO_2$ and PTFE were monitored by EDX elemental mapping across the entire surface of the coatings. Before contact angle measurement, all the coatings were exposed to UV light for 2 h: the contact angle on the coatings was obtained using a sessile drop method with a Dataphysics OCA-20 contact angle analyser (DataPhysics Instruments GmbH, Filderstadt, Germany). The surface energy and its components of the coatings were calculated using the van Oss approach, which have been described in detail previously [34]. X-ray diffraction (XRD) was used to identify crystalline materials. Diffraction patterns were recorded from 3 to 120° 2-$\theta$ using Ni-filtered Cu K-alpha radiation and scanning from 3 to 120° 2-$\theta$ counting for 300 s per step on a Panalytical X-pert Pro diffractometer using an X-celerator position sensitive detector. Mineral phases were identified with reference to patterns in the International Centre for Diffraction Data Powder Diffraction File (PDF).

### 2.3. Anti-adhesive and antibacterial activity

The anti-adhesion efficacy of the $TiO_2$-PTFE coatings was determined by co-culture experiments utilising Gram-negative *Escherichia coli* WT F1693 and Gram-positive *Staphylococcus aureus* F1557 as model bacteria in nutrient media (10% tryptone soya broth (TSB) in phosphate buffered saline (PBS)) (Sigma-Aldrich, UK) at 37 °C. Firstly the stock strains were cultured on tryptone soya agar (TSA) plates overnight at 37 °C. A single colony was then selected and incubated in 5 mL TSB and grown statically overnight at 37 °C. Then, 500 µL of this culture was transferred into 100 mL TSB and grown to the mid-exponential phase, since cells harvested in this growth phase show the best adhesion to a solid surface [35]. Next, $10^6$ CFU/mL *E. coli* and *S. aureus* were prepared in PBS and six replicates of each sample were incubated with 30 mL of the bacterial suspension at 20 rpm at 37 °C. Bacterial adhesion was examined by counting the number of adhered cells at 2, 6, 12 and 24 h, respectively using fluorescence microscopy. A LIVE/DEAD Baclight bacterial viability kit L13152 (Fisher Scientific, UK) was used to stain adhered bacteria, the adhering cells were observed and quantified using a fluorescence microscope (OLYMPUS BX 41, Japan) and Image Pro Plus software (Media Cybernetics, Rockville, USA).

The antibacterial activity of the TiO2-PTFE coatings was evaluated using culture turbidity as a qualitative measure of bacterial growth. All samples were sterilised by autoclaving at 121 °C for 15 min and then added into the above bacterial suspension with UV irradiation (wavelength 254 nm, 4w, Fisher Scientific, UK) for 30 min. Bacterial growth behaviour was examined in the presence of the samples, and growth was monitored at hourly intervals for 12 h at 120 rpm at 37 °C by measuring the increase in optical density (OD) at 600 nm using a spectrophotometer (Biochrom WPA CO8000, Cambridge, UK). All

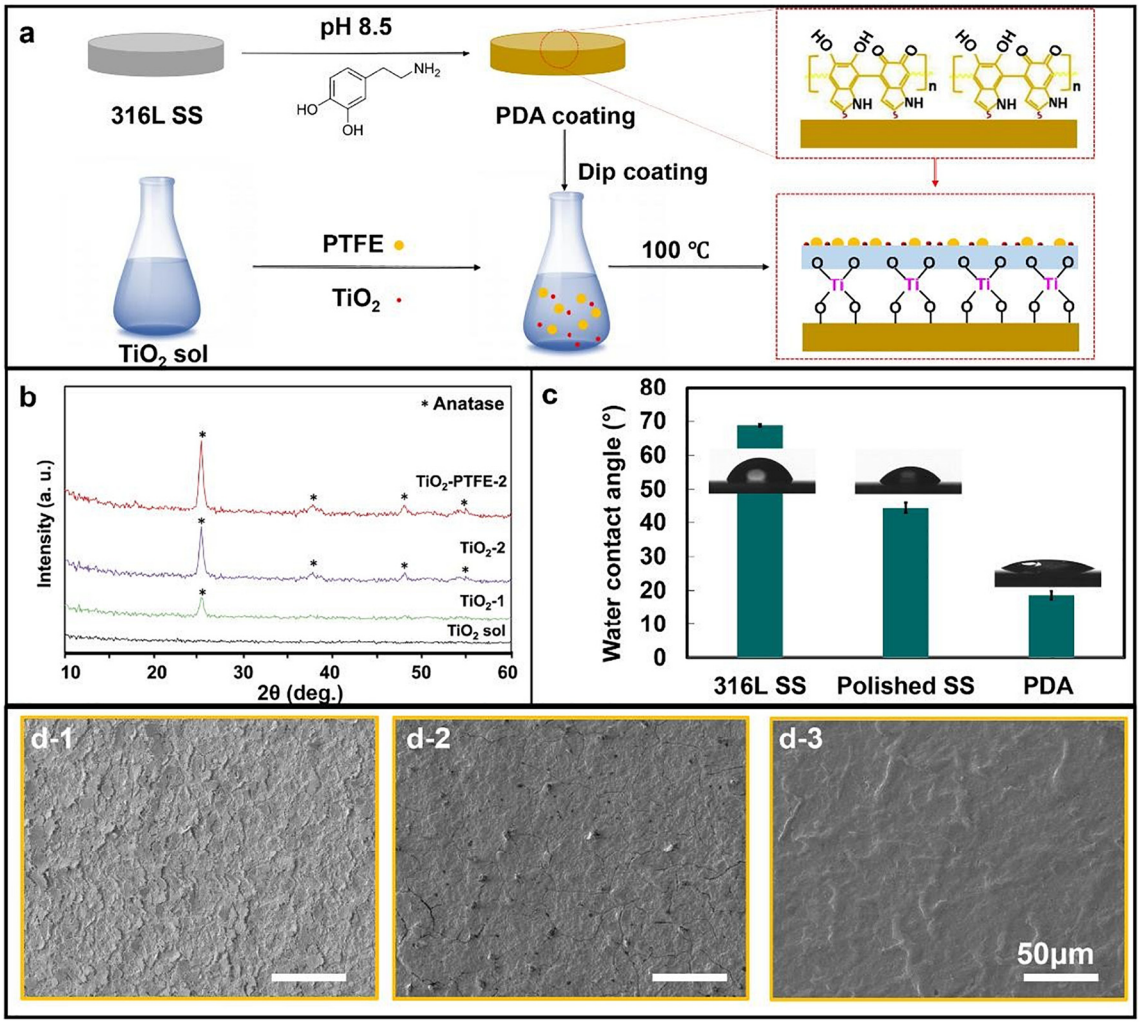


**Fig. 1.** (a) Illustrative diagrams of the $TiO_2$-PTFE coating process; (b) XRD patterns of different coatings; (c) Water contact angles for different substrate surfaces The inserts are images of the water droplets after deposition on the surface for 60 s; (d) SEM images of typical $TiO_2$-PTFE nanocomposite coatings on untreated 316L SS, polished SS and PDA coated surfaces, respectively (all scale bars correspond to 50 μm). Typical data are shown from one of several examinations.

**Table 1**
Contact angle and surface energy components of the coating samples and bacteria ($N$ = 6, bars are standard error of the mean).

| Sample | Particle conc. (g/L) | | Contact angle, $\theta$ (deg) | | | Surface free energy (mJ/m$^2$) | | | |
|---|---|---|---|---|---|---|---|---|---|
| | PTFE | $TiO_2$ | $\theta^W$ | $\theta^D$ | $\theta^E$ | $\gamma^{LW}$ | $\gamma^+$ | $\gamma^-$ | $\gamma^{TOT}$ |
| 316L SS | | | 68.8 ± 0.4 | 36.7 ± 0.1 | 45.0 ± 1.0 | 41.23 | 0.03 | 13.63 | 42.60 |
| PTFE | 2.0 | | 105.8 ± 0.8 | 78.9 ± 0.9 | 89.1 ± 1.3 | 18.06 | 0.00 | 1.58 | 18.21 |
| $TiO_2$-1 | | 1.0 | 48.0 ± 1.3 | 44.1 ± 1.5 | 42.8 ± 0.7 | 37.49 | 0.00 | 40.14 | 37.93 |
| $TiO_2$-2 | | 2.0 | 40.4 ± 1.8 | 43.7 ± 0.9 | 40.7 ± 1.4 | 37.70 | 0.01 | 47.76 | 39.21 |
| $TiO_2$-PTFE-1 | 2.0 | 1.0 | 92.7 ± 1.7 | 64.8 ± 1.5 | 75.6 ± 0.8 | 25.82 | 0.01 | 4.40 | 26.13 |
| $TiO_2$-PTFE-2 | 2.0 | 2.0 | 74.4 ± 2.0 | 56.4 ± 1.3 | 66.9 ± 1.3 | 30.65 | 0.13 | 13.45 | 33.30 |
| *E. coli* [44] | | | 16.5 ± 1.1 | 47.6 ± 0.5 | 22.9 ± 0.7 | 35.60 | 0.14 | 67.68 | 41.76 |
| *S. aureus* [44] | | | 16.6 ± 1.8 | 54.8 ± 0.7 | 22.3 ± 1.2 | 31.56 | 0.43 | 68.32 | 42.40 |

experiments were performed in triplicate.

### 2.4. Corrosion test

The anticorrosion properties of the samples were evaluated electrochemically in vitro using a CorrTest Electrochemistry Workstation with three electrodes: a working electrode, a platinum counter electrode and a saturated calomel (SCE) reference electrode. All measurements were performed in Hank's solution to simulate the biocorrosive environment around an implant [36]. Prior to Tafel polarization, the samples (exposed area: 6.25 $cm_2$) were immersed for 1 h to achieve balanced open circuit potentials (OCP). Potentiodynamic polarization curves (Tafel plots) were recorded from a starting potential of 50 mV below the OCP and scanned towards the positive direction at a scan rate of 0.5 mV/s. Data fitting and analysis were performed using the software CorrTest® 1.2.

### 2.5. Cytotoxicity and cell adhesion

Cytotoxicity tests were performed according to the ISO 10993-

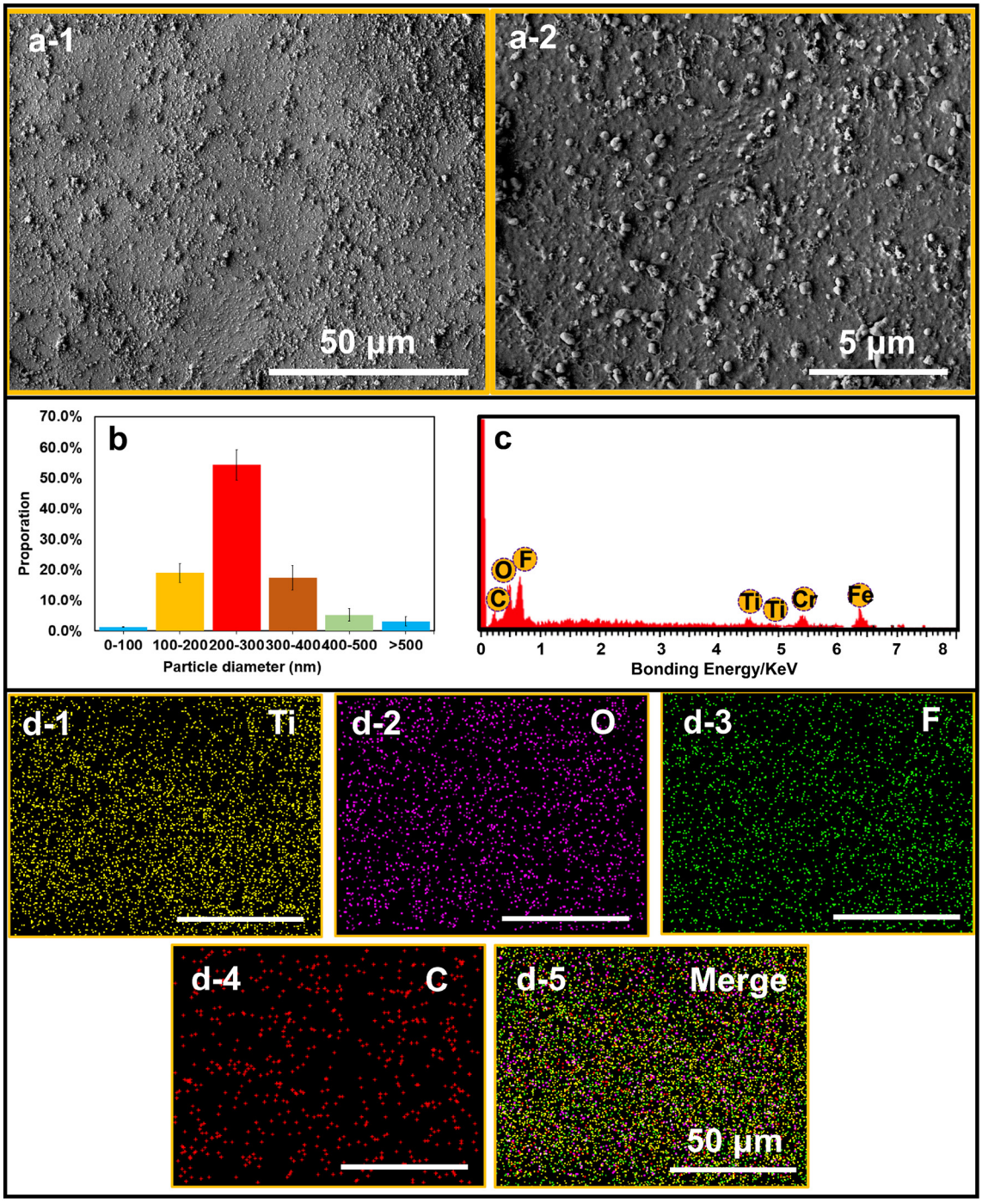


**Fig. 2.** (a) SEM images of $TiO_2$-PTFE nanocomposite coatings at two different magnifications; (b) Size distribution of the PTFE particles; (c) Semi-quantitative results of EDX; (d) EDX mappings of the a-1 SEM image. Typical images are shown from one of several examinations.

5:2009(E), using mouse fibroblast cells L929 obtained from European Collection of Authenticated Cell Cultures (UK) that are commonly used for cytotoxicity evaluation of biomaterials. The L929 cell line was cultured in Eagle's minimum essential medium (MEM) supplemented with 10% fetal bovine serum in addition to 100 mg/mL penicillin and 100 mg/mL streptomycin for 24 h at 37 °C, under air conditioning 5% $CO_2$. After achieving confluence, 500 μL of a cell suspension with ~$10^5$ cells/mL was seeded in each well of a 48-well plate. The cells were then incubated in a humidified atmosphere (> 90% humidity) with 5% $CO_2$ at 37 °C overnight. The samples ($n$ = 6) were carefully placed into the 48 well plate and incubated for 24, 48 and 72 h, respectively. Wells containing only L929 cells were used as control. Cytotoxicity was measured using the 3-(4,5-dimethylthiazol-2-yl)-2,5-diphenyltetrazolium bromide (MTT) assay method. All the medium was removed and 50 μL of MTT was added to each well. After 4 h of incubation in the dark at 37 °C, 500 μL of isopropanol was added to each well to dissolve the formazan. The absorbance was measured at 570 nm and relative cell viability was measured by comparison with the control. In another experiment, L929 cells were plated in a confocal culture dish. As cells reached 30% confluence in all groups, they were treated with the samples for another 72 h. Cells were fixed with 4% paraformaldehyde (PFA) in PBS at 37 °C in the dark overnight and stained with fluorescein Alexa Fluor 488 phalloidin (AF488-phalloidin) (Molecular Probes) and Hoechst 33258 (Molecular Probes). After

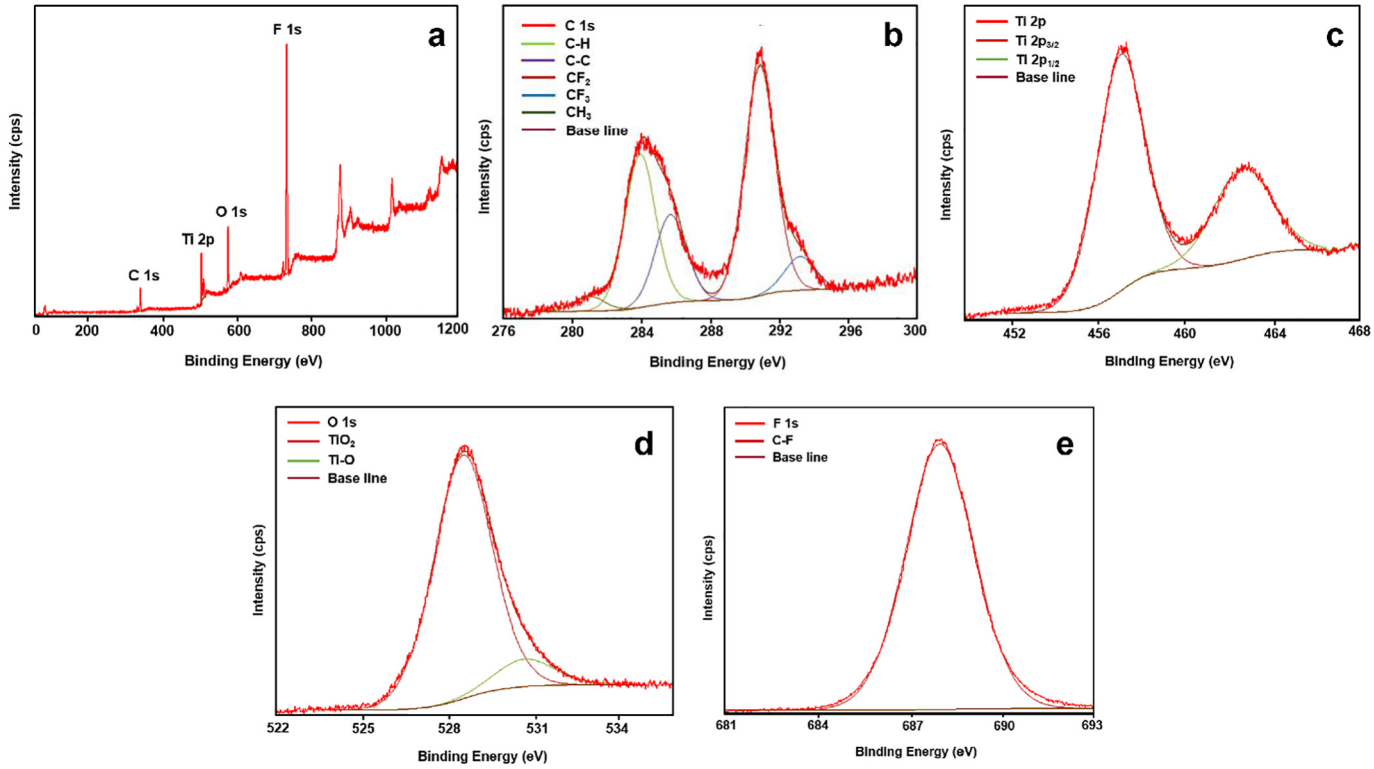


**Fig. 3.** XPS spectra of $TiO_2$-PTFE coatings: (a) wide scan, (b) C 1s, (c) Ti 2p, (d) O 1s and (e) F 1s.

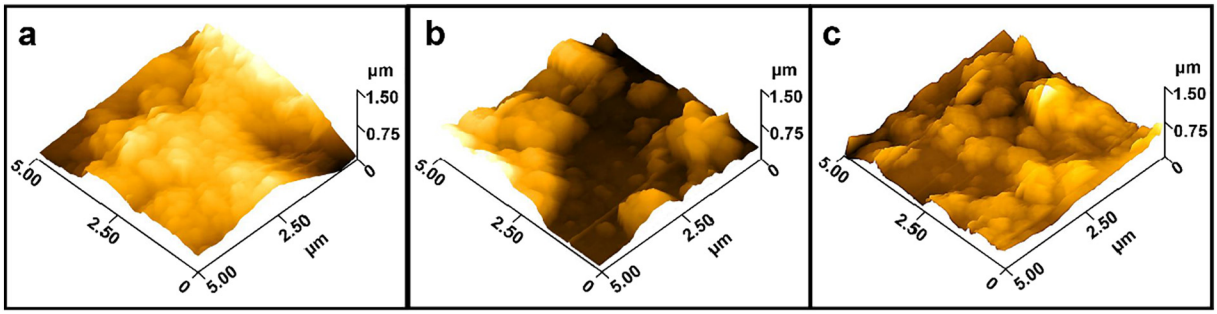


**Fig. 4.** AFM of (a) $TiO_2$-2, (b) PTFE and (c) $TiO_2$-PTFE-2.

incubation with Hoechst 33258, the cells were subsequently washed 3 times in 0.01 M PBS, pH 7.2, before being examined using confocal microscopy (Leica SP8 confocal microscope, Wetzlar, Germany). For examination of cell attachment and spread, samples fixed with 2.5% glutaraldehyde and dehydrated in a graded ethanol series (50–100% (*v/v*), 15 min per step). Samples were then critical point dried using a liquid $CO_2$ BAL-TEC CPD 0.30 critical point dryer (BAL-TEC company, Canonsburg, USA) and subsequently mounted on aluminium stubs using carbon adhesive tape and stored in a desiccator at room temperature. Prior to electron microscopy, samples were coated with 10 nm Au/Pd using a Cressington 208HR sputter coater (Ted Pella, Inc., Redding, CA, USA).

### 2.6. Statistical analysis

Statistical analysis was performed using SPSS software (version 19.0) and data were represented as the means ± standard deviation. Group comparison was conducted using a one-way ANOVA combined with a Student-Newman-Keuls (SNK) post hoc test to determine the level of significance. $p < 0.05$ was considered significant and $p < 0.01$ was considered highly significant.

## 3. Results and discussion

### 3.1. Characterisation of $TiO_2$-PTFE nanocomposite coatings

Although the precise molecular mechanism for dopamine polymerisation has not yet been fully disclosed, the PDA coating was found to be an extremely versatile platform for secondary reactions. Wang et al. [37] demonstrated that PDA could strongly chelate Ti (IV) and $TiO_2$ with OH groups from the catechol binding to Ti molecules to boost nucleation and growth of the $TiO_2$ film. Anderson et al. [38] have also shown that catechol could form bidentate binuclear surface complexes on $TiO_2$ surfaces with covalent and ionic bonding characteristics. Therefore, the PDA sublayer would be chemically bonded rather than being physically adsorbed to the $TiO_2$ sol. In a typical sol-gel $TiO_2$ coating process, the formation of crystalline anatase $TiO_2$ usually requires calcination at over 400 °C [39], but this temperature is much higher than the glass-transition temperature ($T_g$) and melting point of PTFE [40]. Therefore, to synthesise coatings with photocatalytic activity, a range of anatase $TiO_2$ nanoparticles was incorporated into the sol and the $TiO_2$-PTFE coatings were heat treated at 100 °C (Fig. 1a).

As shown in Fig. 1b, the XRD diffraction pattern of the pure $TiO_2$ sol

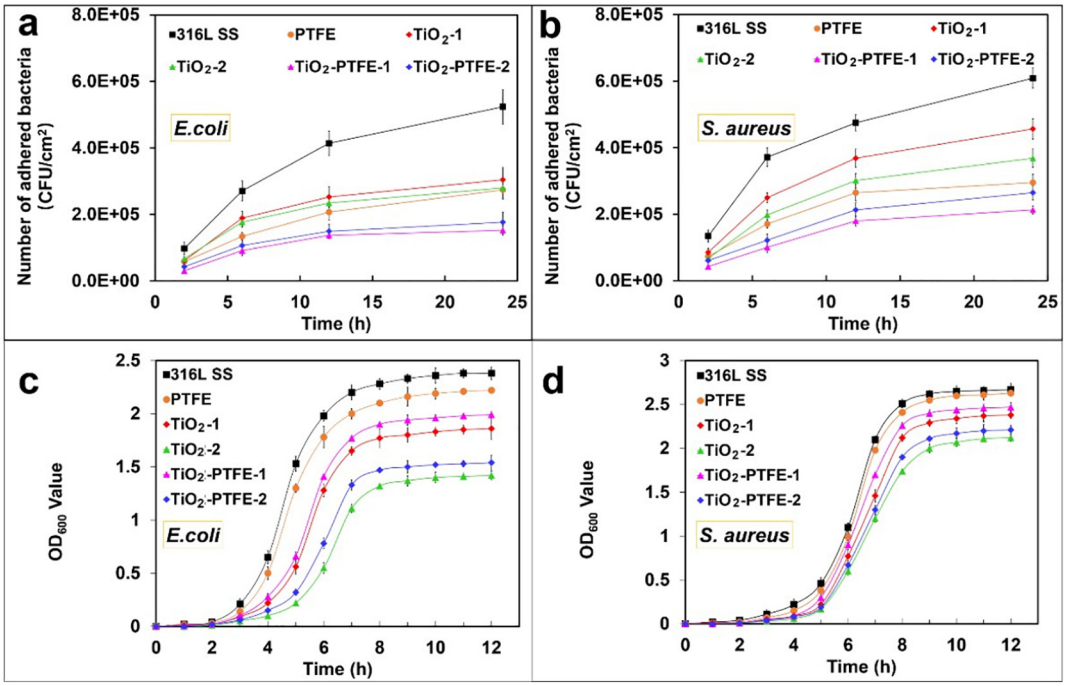


**Fig. 5.** Effect of contact time on adhesion of (a) *E. coli* and (b) *S. aureus* to different samples; bacterial growth in the presence of different samples for (c) *E. coli* and (d) *S. aureus*. ($N$ = 10, bars are standard error of the mean).

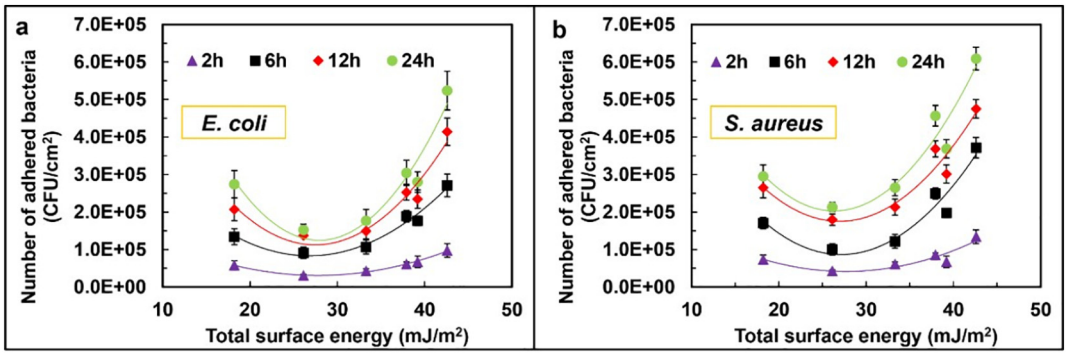


**Fig. 6.** Effect of surface energy on (a) *E. coli* and (b) *S. aureus* adhesion at various contact times ($N$ = 10, bars are standard error of the mean).

did not exhibit clear peaks indicating that the coating without anatase $TiO_2$ incorporation is amorphous in nature. In comparison, the diffraction patterns of $TiO_2$ and $TiO_2$-PTFE coatings (see Fig. 1b and Table 1) showed clear peaks corresponding to the plane of anatase $TiO_2$, which confirms the presence of anatase phase of $TiO_2$ in the coatings. Moreover, the morphology of $TiO_2$-PTFE coated surfaces was also investigated using SEM. The coatings on bare steel substrates showed obvious cracks which could be a result of shrinkage during the thermal process (Fig. 1d-1 and Fig. 1d-2); while after coating with the PDA sublayer, the coating uniformity was significantly improved (Fig. 1d-3). This could be attributed to the improvement of hydrophilicity of the substrate surface that enhances the tendency of the film to resist rupture and lowers the crack propagation velocity [41]. In this study, the hydrophilicity of the substrate surfaces was characterised by measuring the water contact angle (WCA) (Fig. 1c). After polishing and PDA coating, WCA values decreased from 68.8 ± 0.4° (untreated 316L SS) to 44.5 ± 1.6° and 18.6 ± 1.2°, respectively (Fig. 1c).

At higher magnification, the $TiO_2$ nanoparticles and PTFE particles (with an average diameter of 200–300 nm) were uniformly distributed in the coatings (Fig. 2a, b). Fig. 2c shows the typical surface composition of the $TiO_2$-PTFE coating. The major surface constituents included C, O, F, Ti, Cr and Fe. The Fe and Cr were from the 316L SS substrate. Fig. 2d shows the distributions of C, O, F and Ti in the coatings obtained by EDX elemental mapping, which further verifies the uniform distribution of $TiO_2$ and PTFE particles throughout the coating. Fig. 3 shows the XPS results of a typical $TiO_2$-PTFE coating and the wide-scan survey spectrum clearly shows the C 1s, Ti 2p, O 1s and F 1s peaks (Fig. 3a). To identify the existence of PTFE and $TiO_2$, these peaks were separately fitted with several curves. As shown in Fig. 3b and e, typical C-C, C-F, $CF_2$, $CF_3$ groups in PTFE were observed, which confirmed that PTFE particles were successfully incorporated into the coatings. In the core level spectrum of Ti 2p, the binding energies of the peaks were located at 457.0 eV and 462.8 eV, which corresponded to Ti 2p 3/2 and Ti 2p 1/2, respectively (Fig. 3c). The appearances of Ti 2p 3/2 and O1s (at 530.4 eV, Fig. 3d) indicated the $TiO_2$ sol matrix, and the peaks of Ti 2p 1/2 and O1s (at 528.6 eV, Fig. 3d) were attributed to the chemical bonding of $TiO_2$ [24]. Fig. 4 shows the AFM images of $TiO_2$, PTFE and $TiO_2$-PTFE coatings ($TiO_2$, 2.0 g/L, PTFE 2.0 g/L). The surface roughness values (Ra) for the PTFE coatings (141.3 ± 6.9 nm) were much higher than the $TiO_2$ (79.4 ± 9.0 nm) and $TiO_2$-PTFE (129.8 ± 7.7 nm) coatings, which should be ascribed to the large particle size of PTFE (Fig. 2b).

Table 1 shows the water contact angle (WCA) and the surface energy of the coatings. It was found that the concentrations of $TiO_2$ and

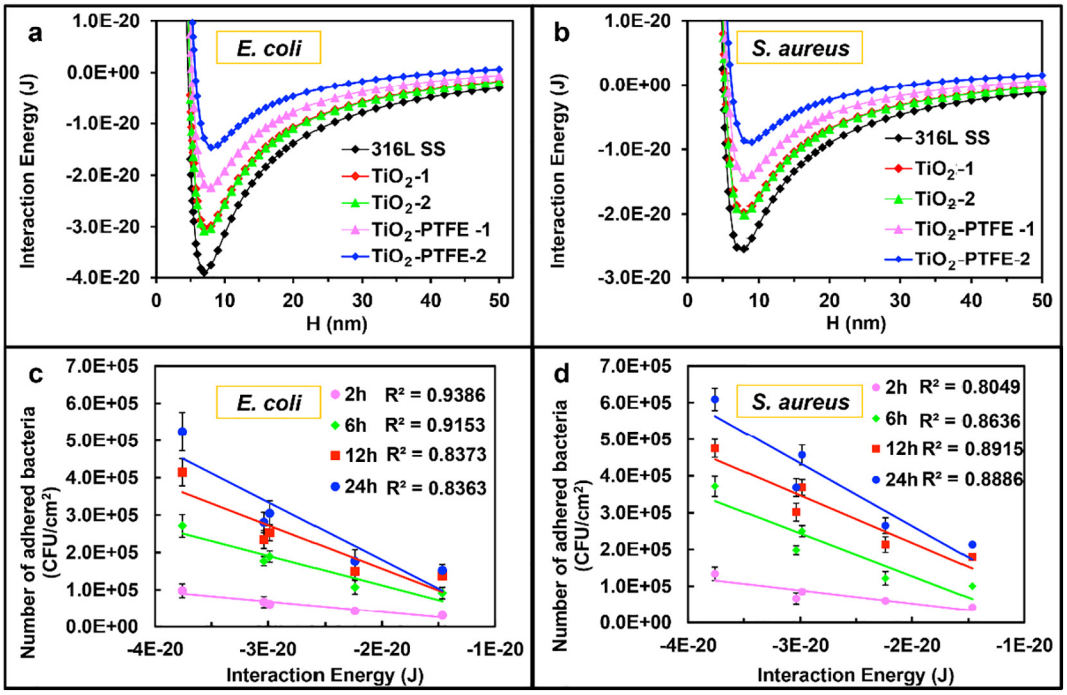


**Fig. 7.** (a–b) Effects of separation distance (H) on interaction energy and (c–d) effects of total interaction energies on bacterial adhesion at 8 nm at different contact times ($N$ = 10, bars are standard error of the mean).

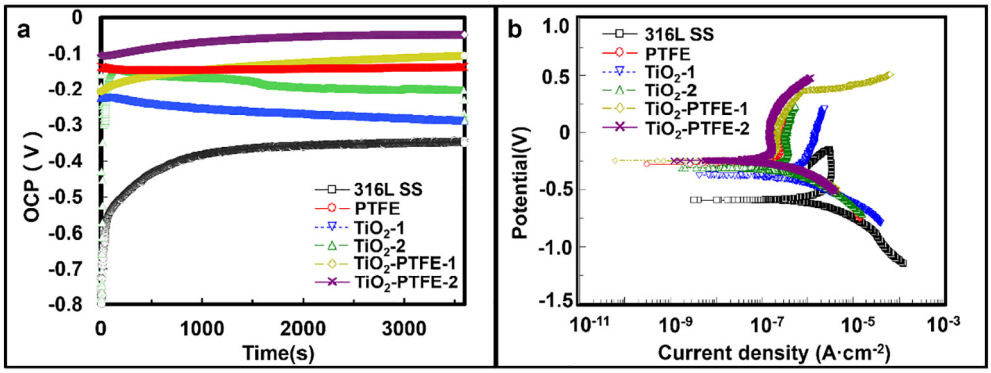


**Fig. 8.** (a) Open-circuit potential characteristics and (b) potentiodynamic polarization curves of different samples in Hank's solution.

**Table 2**
Electrochemical parameters of different samples in Hank's solution.

| Samples | $I_{corr}$ (μA/cm$^2$) | $E_{corr}$ (V) | OCP (V) |
|---|---|---|---|
| 316L SS | 2.77 | −0.59 | −0.35 |
| PTFE | 0.40 | −0.28 | −0.14 |
| $TiO_2$-1 | 1.72 | −0.38 | −0.28 |
| $TiO_2$-2 | 0.56 | −0.31 | −0.23 |
| $TiO_2$-PTFE-1 | 0.34 | −0.25 | −0.11 |
| $TiO_2$-PTFE-2 | 0.21 | −0.22 | −0.05 |

PTFE particles in the coating bath significantly influenced the values of WCA and surface energy of the coatings. Coatings with a PTFE concentration of 2.0 g/L in the bath increased the value of WCA significantly and decreased surface energy components ($\gamma^{LW}$, $\gamma^{-}$ and $\gamma^{TOT}$) due to its hydrophobic and low-surface-energy features. In contrast, an increasing concentration of $TiO_2$ in the coating bath showed an adverse impact. Previous studies have demonstrated that the WCA on $TiO_2$-coated surfaces decreased significantly after UV irradiation [42] and this photo-excitation could further lead to the generation of electron-hole pairs accumulating on the $TiO_2$ surface [43].

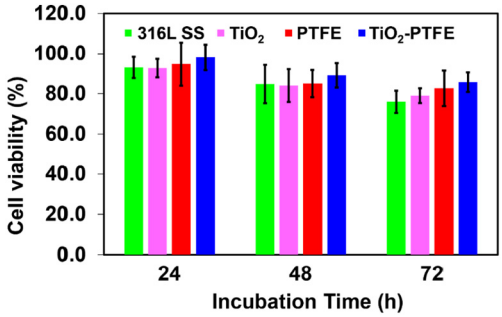


**Fig. 9.** Cell viability (% compared to control) after treatment with different coating samples for 24, 48 and 72 h ($N$ = 6, bars are standard error of the mean).

### 3.2. Bacterial adhesion and growth

As bacterial adhesion and proliferation on medical devices are the chief culprits for hospital infections, the adhesion of two common potential pathogens (Gram-negative *E. coli* and Gram-positive *S. aureus*) to

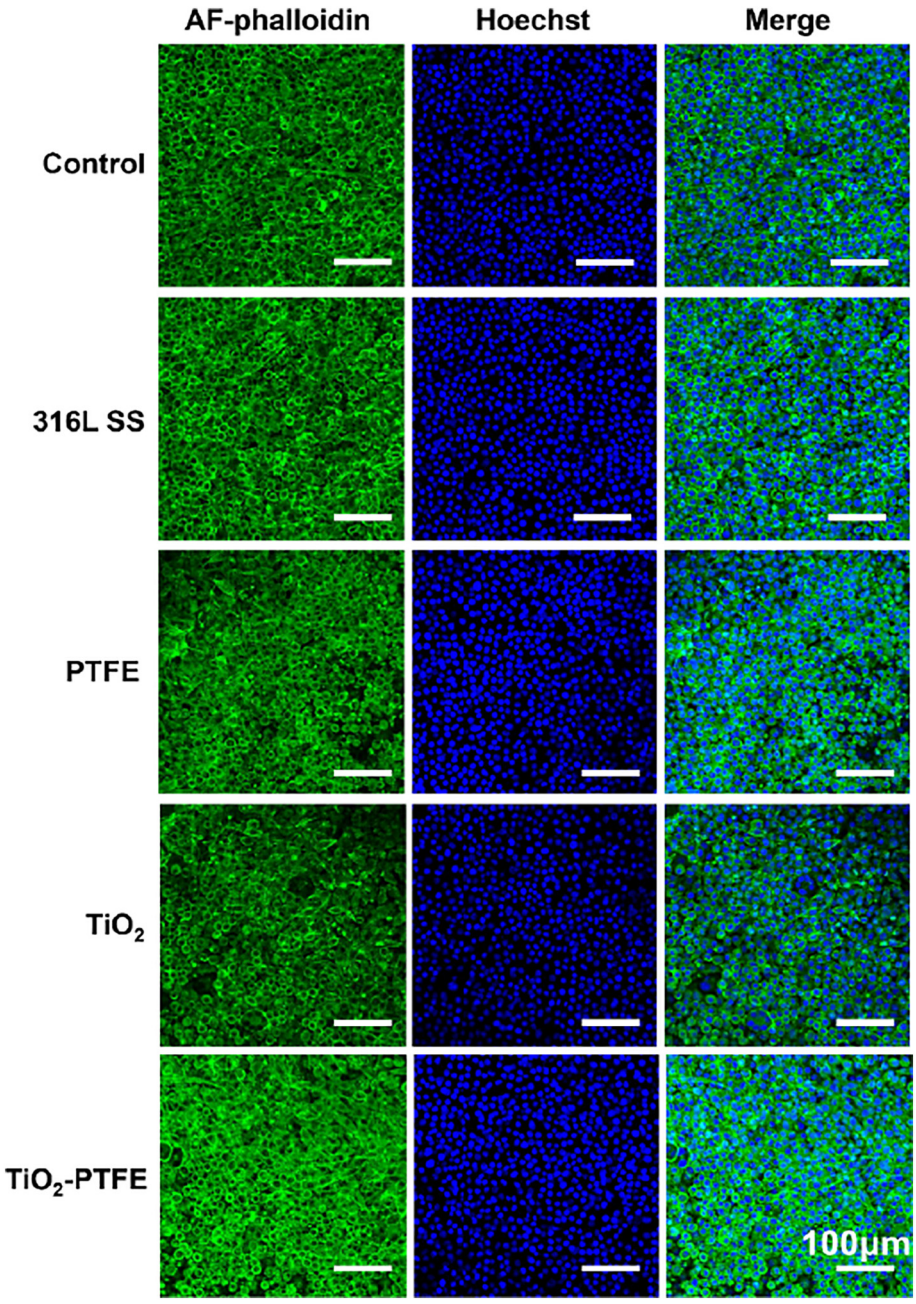


**Fig. 10.** Confocal microscopy images of fibroblast cells after 72 h of treatment with different coating samples (scale bar corresponds to 100 μm). Typical images are shown from one of several examinations.

the coatings was evaluated using fluorescence microscopy after contact times of 2, 6, 12 and 24 h. Generally, the number of adhering bacteria increased with increasing contact time for all coatings (Fig. 5a and b). The $TiO_2$-PTFE-1 coated surface exhibited the lowest bacterial adherence, reducing adhesion of *E. coli* and *S. aureus* by 70.9% and 65.0%, respectively, after 24 h, as compared with the uncoated 316L SS surface.

Fig. 5c and d show the results for *E. coli* and *S. aureus,* respectively. The bacteria cultured with PTFE coated samples showed similar growth to the control over the test period. In comparison, the $TiO_2$-containing samples ($TiO_2$-1, $TiO_2$-2, $TiO_2$-PTFE-1 and $TiO_2$-PTFE-2) exhibited noticeable inhibition of bacterial growth. The bacterial inhibition increased with increasing $TiO_2$ concentration in the bath (see Table 1). For a given $TiO_2$ concentration in the bath, the $TiO_2$ coatings performed slightly better than the $TiO_2$-PTFE coatings. A difference in the inhibition effects was also observed between the two strains. Li et al. [45] reported that although $TiO_2$ can kill both Gram-negative and Gram-positive bacteria, Gram-positive bacteria are less sensitive due to their thicker cell wall.

### 3.3. Effect of surface energy on bacterial adhesion

The influence of surface energy on bacterial adhesion has been investigated extensively with the frequent conclusion that low-energy surfaces are less prone to bacterial adhesion due to weaker binding at the interface [46]. In this study, a range of coatings with total surface energy from 18.21 $mJ/m^2$ to 42.60 $mJ/m^2$ were prepared and the effects of surface energy on adhesion of *E. coli* and *S. aureus* were studied after different contact times. As shown in Fig. 6, the $TiO_2$-PTFE-1 coated surface with the surface energy 26.13 $mJ/m^2$ performed best against

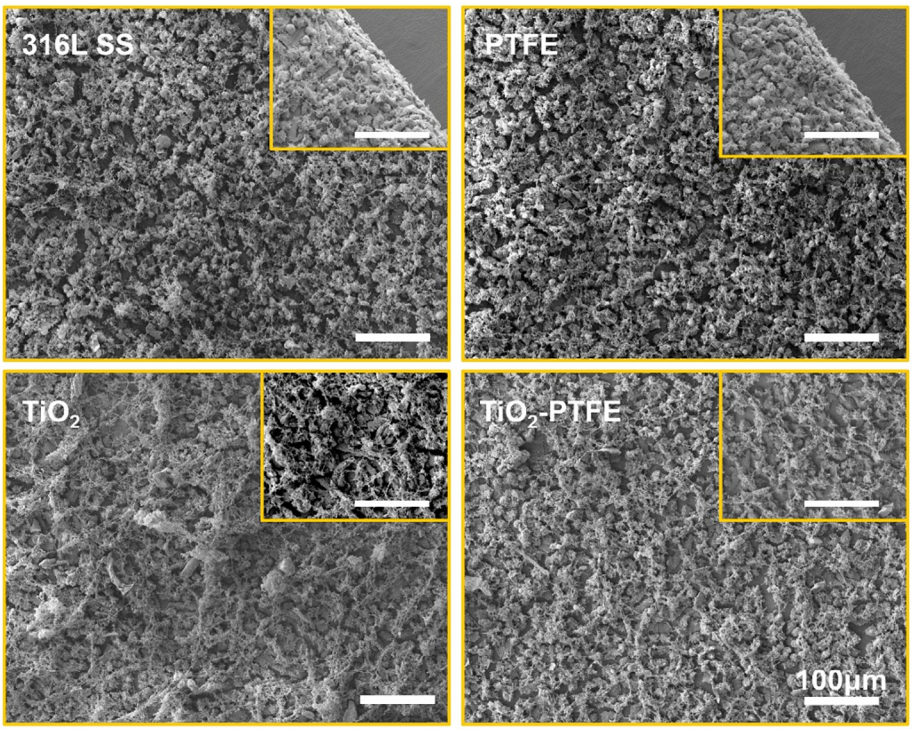


**Fig. 11.** SEM observations of L929 mouse fibroblasts after incubation with different surfaces for 72 h (all scale bars correspond to 10 μm.) Typical images are shown from one of several examinations.

bacterial adhesion at all contact times. The results also showed that there existed an optimal value for the surface energy (between 20 and 30 mJ/m$^2$) at which bacterial adhesion is minimal. These results were consistent with the Baier curve [47].

Bacterial adhesion is a complicated process that is influenced by numerous factors such as properties of bacteria, substratum surface and fluid [48]. The most prominent model for quantitative prediction of bacteria-material interaction energies is the extended Derjaguin-Landau-Verwey-Overbeek (DLVO) theory [49]. The principal interaction forces determining hetero-coagulation include a Lifshitz–van der Waals (LW) interactive component, an electrostatic double-layer (EL) component, a Lewis acid-base (AB) component, and Brownian motion (Br) [49]. The total interaction energy $\Delta E^{TOT}$ between bacteria 1 and a solid surface 2 in a fluid 3 can be written as the sum of these corresponding interaction terms [49]:

$$\Delta E^{TOT} = \Delta E_{132}^{LW} + \Delta E_{132}^{EL} + \Delta E_{132}^{AB} + \Delta E_{132}^{Br} \quad (1)$$

The balance between all possible interactions determines whether or not the bacteria will attach on the surface: adhesion will take place when $\Delta E^{TOT}$ is negative. In this model, all these interactions are dependent on the distance of separation (H) between the interacting entities (i.e. the bacteria and solid surfaces). Bacterial cells can fall into a deep primary energy minimum at close contact and adhere irreversibly [50]. In this study, the interaction energy $\Delta E^{TOT}$ as a function of separation distance (H) was calculated according to our previous studies [25,51,52]. As shown in Fig. 7a and b, the values of interaction energy reached a minimum when the separation distance was about 8 nm. The minimal total interaction energies were then calculated and their effects on bacterial adhesion were also assessed. Fig. 7c and d show a strong correlation between the total interaction energy $\Delta E^{TOT}$ at H = 8 nm and bacterial adhesion. The number of adhered cells decreased linearly with increasing total interaction energy $\Delta E^{TOT}$, which is consistent with the extended DLVO theory.

### 3.4. Corrosion resistance

For metallic implants, corrosion is almost inevitable and is responsible for prosthesis instability and potential toxicity to the host. Although stainless steels remain popular for implant applications due to their excellent fabrication properties, low cost, accepted biocompatibility and strength, 316L stainless steel contains significant amounts of chromium (16–18%) and nickel (10–14%). The release of these metals into human tissue and fluids must be regarded as a likely source of long-term problems owing to their known potential carcinogenic and toxic effects [53]. However, this could be avoided or alleviated through improving the anti-corrosion properties of the materials. In this study, the corrosion resistance of the coatings was determined via an electrochemical method. As shown in Fig. 8a, after coating, all the OCP values of the samples shifted positively: the final potentials after 1 h are shown in Table 2. The OCP shift in the noble direction suggested the formation of a passive film that acted as a barrier for metal dissolution and reduced the corrosion rate. The $TiO_2$-PTFE-2 coating had the highest OCP value indicating the best thermodynamic stability. From the Tafel plots (Fig. 8b, Table 2), all the coated samples demonstrated a more positive corrosion potential ($E_{corr}$) and a lower corrosion current density ($I_{corr}$). In particular, the $TiO_2$-PTFE-2 coating exhibited the best substrate protection by decreasing the $I_{corr}$ of 316L SS by more than one order of magnitude. These results also demonstrated that the combination of $TiO_2$ and PTFE in coatings resulted in a synergistic effect in improving corrosion resistance, compared to the pure $TiO_2$ or PTFE coatings.

### 3.5. Cytotoxicity assay

The biocompatibility of a coating material is an essential aspect with regard to potential clinical translation and cell culture studies are usually the first step to investigate the potential toxicity of these coatings [54]. In this study, the cytotoxicity of the samples to L929 mouse fibroblast cells was examined using a direct contact method. Firstly, the inhibition ability of coatings to the growth of fibroblast cells was

investigated by the MTT assay. As shown in Fig. 9, following 24 h of co-incubation, cell growth was not inhibited by 316L SS (93.0%), PTFE (94.7%), $TiO_2$ (92.7%), or $TiO_2$-PTFE coated samples (98.1%). As the incubation time increased, the cell viability for all samples showed a slight decrease. Interestingly, after 72 h incubation, the biocompatibility of the samples showed a similar order to that found for corrosion resistance, i.e. $TiO_2$-PTFE > PTFE > $TiO_2$ > 316L SS, indicating the coatings combining $TiO_2$ and PTFE not only improved the corrosion resistance but also the biocompatibility.

The morphologies of L929 cells cultured with samples for 72 h were also investigated by confocal microscopy. As displayed in Fig. 10, there was no significant difference in cell morphology between samples. In order to further investigate cell adhesion on the coatings, cell morphologies on samples were visualised using SEM after 72 h incubation (Fig. 11). It was found that all the samples were coated with a vast number of fibroblast cells with the cells being distributed homogeneously and adhering tightly to surfaces with dense filopodia which could be beneficial to cell proliferation. Moreover, cells on all the surfaces tended to spread with a healthy flattened shape. These results further confirmed that the $TiO_2$-PTFE coating had no toxicity towards the fibroblast cell, making it a promising candidate as an antibacterial and anti-corrosion coating for metallic implants.

## 4. Conclusion

In this research, we have demonstrated a facile and cost-effective approach to produce $TiO_2$-PTFE coatings for metallic implants by combining a sol-gel coating technique and mussel-inspired surface functionalisation. The PDA intermediate layer significantly enhanced the hydrophilicity of the substrate which further improved the coating uniformity. The antibacterial and anti-adhesion properties against the Gram-negative *E. coli* and Gram-positive *S. aureus* relied on the synergistic effect between $TiO_2$ and PTFE. The UV-activated $TiO_2$ nanoparticles can inhibit bacterial growth and the surface energy of the coatings can be modified to reduce bacterial adhesion by controlling the PTFE and $TiO_2$ contents. The $TiO_2$-PTFE coatings were also proved to have excellent corrosion resistance in Hank's solution and demonstrated improved biocompatibility as compared to the bare 316 LSS. Further investigations are required to confirm the anti-infection effects in clinical trials. The positive results obtained in this study make the $TiO_2$-PTFE coating a promising candidate for the development of novel antibacterial and anti-corrosion coatings for metallic implants in the future.

## Declaration of Competing Interests

The authors declare no conflict of interests.

## Acknowledgement

The authors acknowledge the financial supports from the UK Engineering and Physical Sciences Research Council (EP/P00301X/1).

## References

[1] K. Prasad, O. Bazaka, M. Chua, M. Rochford, L. Fedrick, J. Spoor, R. Symes, M. Tieppo, C. Collins, A. Cao, D. Markwell, K.K. Ostrikov, K. Bazaka, Metallic biomaterials: current challenges and opportunities, Materials 10 (2017) 884.
[2] Z.W. Teo Wendy, P.C. Schalock, Hypersensitivity reactions to implanted metal devices: facts and fictions, J Investig Allergol Clin Immunol 26 (2016) 279–294.
[3] A.G. Ashbaugh, X. Jiang, J. Zheng, A.S. Tsai, W.S. Kim, J.M. Thompson, R.J. Miller, J.H. Shahbazian, Y. Wang, C.A. Dillen, A.A. Ordonez, Y.S. Chang, S.K. Jain, L.C. Jones, R.S. Sterling, H.Q. Mao, L.S. Miller, Polymeric nanofiber coating with tunable combinatorial antibiotic delivery prevents biofilm-associated infection in vivo, Proc. Natl. Acad. Sci. USA 113 (2016) 6919–6928.
[4] A.J. van der Borden, P.G. Maathuis, E. Engels, G. Rakhorst, H.C. van der Mei, H.J. Busscher, P.K. Sharma, Prevention of pin tract infection in external stainless-steel fixator frames using electric current in a goat model, Biomaterials 28 (2007) 2122–2126.
[5] T.P. Schaer, S. Stewart, B.B. Hsu, A.M. Klibanov, Hydrophobic polycationic coatings that inhibit biofilms and support bone healing during infection, Biomaterials 33 (2012) 1245–1254.
[6] D. Gil, S. Shuvaev, A. Frank-Kamenetskii, V. Reukov, C. Gross, A. Vertegel, Novel antibacterial coating on orthopaedic wires to eliminate pin tract infections, Antimicrob. Agents Chemother. 61 (2017) (e00442-17).
[7] W. Chen, Y. Liu, H.S. Courtney, M. Betteng, C.M. Agrawal, J.D. Bumgardner, J.L. Ong, In vitro anti-bacterial and biological properties of magnetron co-sputtered silver-containing hydroxyapatite coating, Biomaterials 27 (2006) 5512–5517.
[8] R.O. Darouiche, H. Safar, I.I. Raad, In vitro efficacy of antimicrobial-coated bladder catheters in inhibiting bacterial migration along catheter surface, J. Infect. Dis. 176 (1997) 1109–1112.
[9] D. Li, P. Lv, L. Fan, Y. Huang, F. Yang, X. Mei, D. Wu, The immobilization of antibiotic-loaded polymeric coatings on osteoarticular Ti implants for the prevention of bone infections, Biomater. Sci. 5 (2017) 2337–2346.
[10] R. Chen, M.D. Willcox, K.K. Ho, D. Smyth, N. Kumar, Antimicrobial peptide melamine coating for titanium and its in vivo antibacterial activity in rodent subcutaneous infection models, Biomaterials 85 (2016) 142–151.
[11] D. McShan, P.C. Ray, H. Yu, Molecular toxicity mechanism of nanosilver, J. Food Drug Anal. 22 (2014) 116–127.
[12] H. Qu, C. Knabe, S. Radin, J. Garino, P. Ducheyne, Percutaneous external fixator pins with bactericidal micron-thin sol-gel films for the prevention of pin tract infection, Biomaterials 62 (2015) 95–105.
[13] K. Soontornvipart, A. Nečas, M. Dvořák, Effects of metallic implant on the risk of bacterial osteomyelitis in small animals, Acta. Vet. Brno. 72 (2003) 235–247.
[14] J.L. Gilbert, S. Sivan, Y. Liu, S.B. Kocagöz, C.M. Arnholt, S.M. Kurtz, Direct in vivo inflammatory cell-induced corrosion of CoCrMo alloy orthopaedic implant surfaces, J. Biomed. Mater. Res. A 103 (2015) 211–223.
[15] Q. Chen, G.A. Thouas, Metallic implant biomaterials, Mater. Sci. Eng. R. Rep. 87 (2015) 1–57.
[16] S. Habibzadeh, L. Li, D.S. Timc, E.C. Davis, S. Omanovic, Electrochemical polishing as a 316L stainless steel surface treatment method: towards the improvement of biocompatibility, Corros. Sci. 87 (2014) 89–100.
[17] T. Verdier, M. Coutand, A. Bertron, C. Roques, Antibacterial activity of $TiO_2$ photocatalyst alone or in coatings on E. coli: the influence of methodological aspects, Coatings 4 (2014) 670–686.
[18] X. He, G. Zhang, X. Wang, R. Hang, X. Huang, L. Q, B. Tang, X. Zhang, Biocompatibility, corrosion resistance and antibacterial activity of $TiO_2$/CuO coating on titanium, Ceram. Int. 43 (2017) 16185–16195.
[19] Y. Huang, W. Wang, X. Zhang, X. Liu, Z. Xu, S. Han, Z. Su, H. Liu, Y. Gao, H. Yang, A prospective material for orthopedic applications: Ti substrates coated with a composite coating of a titania-nanotubes layer and a silver-manganese-doped hydroxyapatite layer, Ceram. Int. 44 (2018) 5528–5542.
[20] Y. Huang, G. Song, X. Chang, Z. Wang, X. Zhang, S. Han, Z. Su, H. Yang, D. Yang, X. Zhang, Nanostructured $ag^+$-substituted fluorhydroxyapatite-$TiO_2$ coatings for enhanced bactericidal effects and osteoinductivity of Ti for biomedical applications, Int. J. Nanomedicine 13 (2018) 2665–2684.
[21] G. Carré, E. Hamon, S. Ennahar, M. Estner, M.C. Lett, P. Horvatovich, J.P. Gies, V. Keller, N. Keller, P. Andre, $TiO_2$ photocatalysis damages lipids and proteins in Escherichia coli, Appl. Environ. Microbiol. 80 (2014) 2573–2581.
[22] P.C. Maness, S. Smolinski, D.M. Blake, Z. Huang, E.J. Wolfrum, W.A. Jacoby, Bactericidal activity of photocatalytic $TiO_2$ reaction: toward an understanding of its killing mechanism, Appl. Environ. Microbiol. 65 (1999) 4094–4098.
[23] Y. Ohko, Y. Utsumi, C. Niwa, T. Tatsuma, K. Kobayakawa, Y. Satoh, Y. Kubota, A. Fujishima, Self-sterilizing and self-cleaning of silicone catheters coated with $TiO_2$ photocatalyst thin films: a preclinical work, J. Biomed. Mater. Res. 58 (2001) 97–101.
[24] C. Liu, L. Geng, Y. Yu, Y. Zhang, B. Zhao, Q. Zhao, Mechanisms of the enhanced antibacterial effect of Ag-$TiO_2$ coatings, Biofouling 34 (2018) 190–199.
[25] C. Liu, Q. Zhao, Influence of surface-energy components of Ni-P-$TiO_2$-PTFE nanocomposite coatings on bacterial adhesion, Langmuir 27 (2011) 9512–9519.
[26] C. Liu, L. Geng, Y. Yu, Y. Zhang, B. Zhao, S. Zhang, Q. Zhao, Reduction of bacterial adhesion on Ag-$TiO_2$ coatings, Mater. Lett. 218 (2018) 334–336.
[27] Q. Zhao, C. Liu, X. Su, S. Zhang, W. Song, S. Wang, G. Ning, J. Ye, Y. Lin, W. Gong, Antibacterial characteristics of electroless plating Ni-P-$TiO_2$ coatings, Appl. Surf. Sci. 274 (2013) 101–104.
[28] C. Liu, Q. Zhao, The CQ ratio of surface energy components influences adhesion and removal of fouling bacteria, Biofouling 27 (2011) 275–285.
[29] Q. Zhao, Y. Liu, C. Wang, Development and evaluation of electroless Ag-PTFE composite coatings with anti-microbial and anti-corrosion properties, Appl. Surf. Sci. 252 (2005) 1620–1627.
[30] Q. Zhao, Effect of surface free energy of graded Ni-P-PTFE coatings on bacterial adhesion, Surf. Coat. Technol. 185 (2004) 199–204.
[31] Q. Zhao, Y. Liu, Modification of stainless steel surfaces by electroless Ni-P and small amount of PTFE to minimize bacterial adhesion, J. Food Eng. 72 (2006) 266–272.
[32] Y. Zhang, W. Wang, X. Ma, L. Jia, Polydopamine assisted fabrication of titanium oxide nanoparticles modified column for proteins separation by capillary electrochromatography, Anal. Biochem. 512 (2016) 103–109.
[33] H. Lee, S.M. Dellatore, W.M. Miller, P.B. Messersmith, Mussel-inspired surface chemistry for multifunctional coatings, Science 318 (2007) 426–430.
[34] C. Liu, Q. Zhao, Y. Liu, S. Wang, E.W. Abel, Reduction of bacterial adhesion on modified DLC coatings, Colloids Surf. B 61 (2008) 182–187.
[35] Y. Zhao, B. Zhao, X. Su, S. Zhang, S. Wang, R. Keatch, Q. Zhao, Reduction of bacterial adhesion on titanium-doped diamond-like carbon coatings, Biofouling 34 (2018) 26–33.
[36] Z. Jia, P. Xiu, M. Li, X. Xu, Y. Shi, Y. Cheng, S. Wei, Y. Zheng, T. Xi, H. Cai, Z. Liu,

Bioinspired anchoring AgNPs onto micro-nanoporous $TiO_2$ orthopedic coatings: trap-killing of bacteria, surface-regulated osteoblast functions and host responses, Biomaterials 75 (2016) 203–222.
[37] Z. Wang, J. Li, F. Tang, J. Lin, Z. Jin, Polydopamine nanotubes-templated synthesis of $TiO_2$ and its photocatalytic performance under visible light, RSC Adv. 7 (2017) 23535–23542.
[38] T.H. Anderson, J. Yu, A. Estrada, M.U. Hammer, J.H. Waite, J.N. Israelachvili, The contribution of DOPA to substrate–peptide adhesion and internal cohesion of mussel-inspired synthetic peptide films, Adv. Funct. Mater. 20 (2010) 4196–4205.
[39] D.J. Kim, S.H. Hahn, S.H. Oh, E.J. Kim, Influence of calcination temperature on structural and optical properties of $TiO_2$ thin films prepared by sol-gel dip coating, Mater. Lett. 57 (2002) 355–360.
[40] P.J. Rae, D.M. Dattelbaum, The properties of poly(tetrafluoroethylene) (PTFE) in compression, Polymer 45 (2004) 7615–7625.
[41] U.U. Ghosh, M. Chakraborty, A.B. Bhandari, S. Chakraborty, S. DasGupta, Effect of surface wettability on crack dynamics and morphology of colloidal films, Langmuir 31 (2015) 6001–6010.
[42] B. Li, B.E. Logan, The impact of ultraviolet light on bacterial adhesion to glass and metal oxide-coated surface, Colloids Surf. B 41 (2005) 153–161.
[43] S. Anandan, Y. Ikuma, K. Niwa, An overview of semi-conductor photocatalysis: modification of $TiO_2$ nanomaterials, Solid State Phenom. 162 (2010) 239–260.
[44] X. Su, Development and Evaluation of Anti-biofouling Nanocomposite Coatings (Doctoral Thesis), University of Dundee, 2013, https://discovery.dundee.ac.uk/ws/portalfiles/portal/2280998/Su_phd_2013.pdf.
[45] Q. Li, S. Mahendra, D.Y. Lyon, L. Brunet, M.V. Liga, D. Li, P.J. Alvarez, Antimicrobial nanomaterials for water disinfection and microbial control: potential applications and implications, Water Res. 42 (2008) 4591–4602.
[46] Q. Zhao, Y. Liu, C. Wang, S. Wang, H. Müller-Steinhagen, Effect of surface free energy on the adhesion of biofouling and crystalline fouling, Chem. Eng. Sci. 60 (2005) 4858–4865.
[47] R.E. Baier, Surface behaviour of biomaterials: the theta surface for biocompatibility, J Mater. Sci. Mater. Med. 17 (2006) 1057–1062.
[48] M. Katsikogianni, Y.F. Missirlis, Concise review of mechanisms of bacterial adhesion to biomaterials and of techniques used in estimating bacteria-material interactions, Eur. Cell Mater. 8 (2004) 37–57.
[49] M. Hermansson, The DLVO theory in microbial adhesion, Colloids Surf. B 14 (1999) 105–119.
[50] S. Bayoudh, A. Othmane, L. Mora, H.B. Ouada, Assessing bacterial adhesion using DLVO and XDLVO theories and the jet impingement technique, Colloids Surf. B 73 (2009) 1–9.
[51] W. Shao, Q. Zhao, Effect of corrosion rate and surface energy of silver coatings on bacterial adhesion, Colloids Surf. B 76 (2010) 98–103.
[52] D.W. Ren, Q. Zhao, A. Bendavid, Anti-bacterial property of Si and F doped diamond-like carbon coatings, Surf. Coat. Technol. 226 (2013) 1–6.
[53] K. Bordji, J.Y. Jouzeau, D. Mainard, Evaluation of the effect of three surface treatments on the biocompatibility of 316L stainless steel using human differentiated cells, Biomaterials 17 (1996) 491–500.
[54] K.G. Ozdemir, H. Yilmaz, S. Yilmaz, In vitro evaluation of cytotoxicity of soft lining materials on L929 cells by MTT assay, J Biomed Mater Res B Appl Biomater 90 (2009) 82–86.